The novelties and research highlights of this work are briefly summarized below:

- A detailed experimental procedure has been developed for the synthesis of aliphatic urethane-based shape memory polymers (SMPs).
- Comprehensive thermomechanical characterizations on a variety of SMP compositions have been performed to investigate the key connections between the polymer's working temperature, thermal stability and their mechanical behavior.
- Recovery tests have also been conducted for demonstrating the superb shape memory and recovering features of the SMPs which is desirable for the endovascular embolization procedure.
- A range of SMP compositions that most accurately meet our criteria have been identified in this study with their great potential for the individualized treatment of intracranial aneurysms, which will be analyzed further in more detail as a part of future studies.

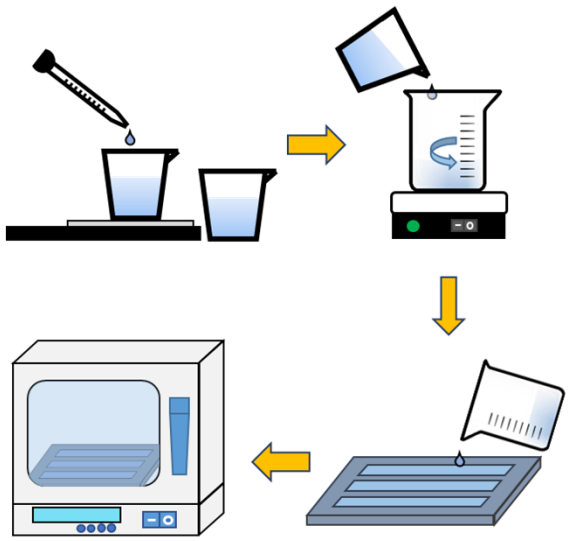

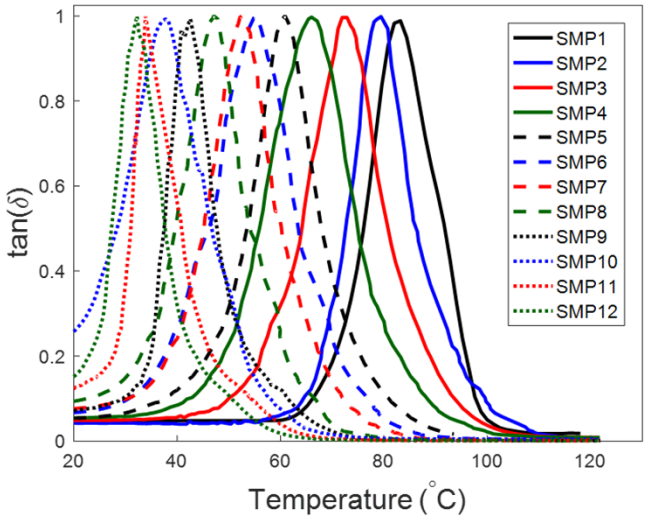
tan(δ)
Temperature (°C)
SMP1
SMP2
SMP3
SMP4
SMP5
SMP6
SMP7
SMP8
SMP9
SMP10
SMP11
SMP12

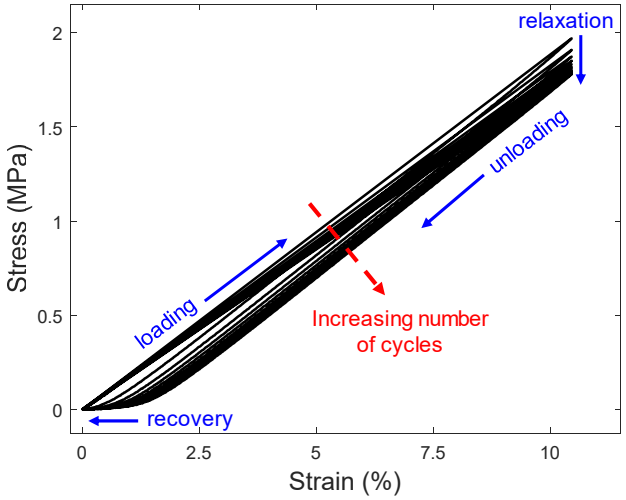
Stress (MPa)
Strain (%)
relaxation
unloading
loading
recovery
Increasing number
of cycles

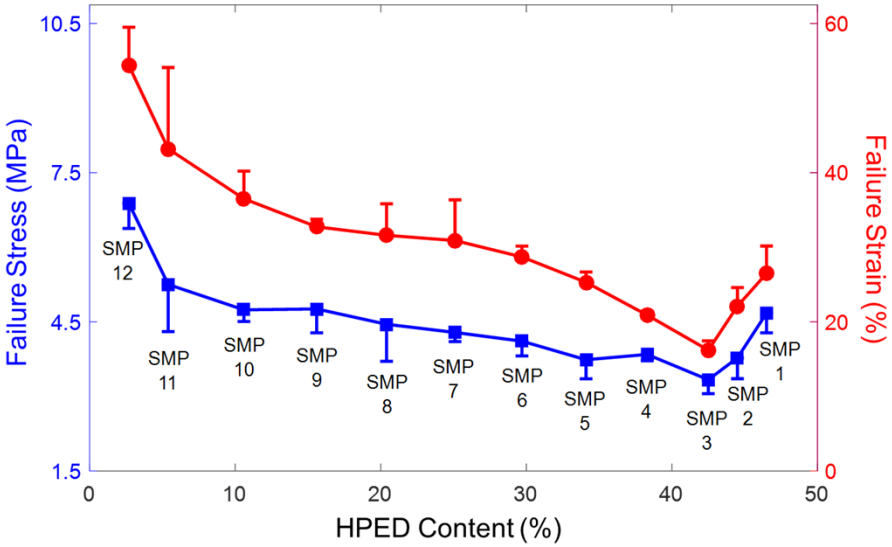
Failure Stress (MPa)
Failure Strain (%)
HPED Content (%)
SMP 12
SMP 11
SMP 10
SMP 9
SMP 8
SMP 7
SMP 6
SMP 5
SMP 4
SMP 3
SMP 2
SMP 1

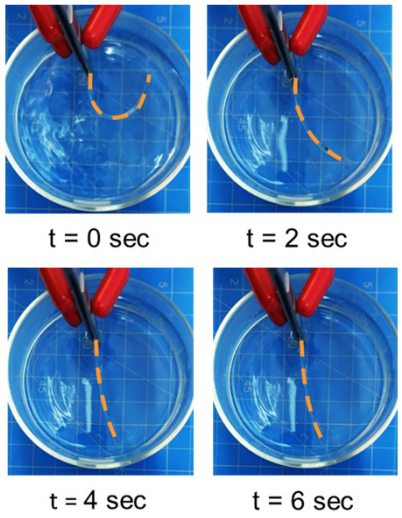
t = 0 sec
t = 2 sec
t = 4 sec
t = 6 sec

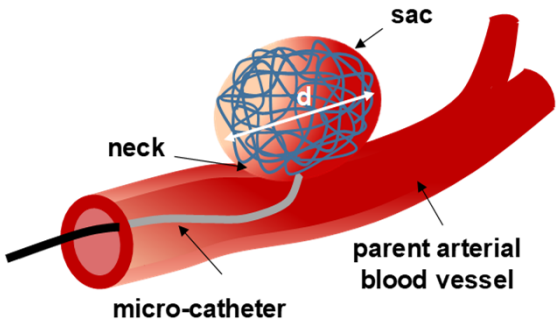
sac
d
neck
parent arterial
blood vessel
micro-catheter

Synthesis and characterization of bio-compatible shape memory polymers with potential applications to endovascular embolization of intracranial aneurysms

Robert Kunkel[1], Devin Laurence[1*], Jingyu Wang[1], Donnie Robinson[1], Joshua Scherrer[1], Yi Wu[1], Bradley N. Bohnstedt[2], Aichi Chien[3], Yingtao Liu[1], and Chung-Hao Lee[1,4]

[1]School of Aerospace and Mechanical Engineering
The University of Oklahoma
Norman, OK 73019, USA

[2]Department of Neurosurgery
The University of Oklahoma Health Sciences Center
Oklahoma City, OK 73104, USA

[3]Division of Interventional Neuroradiology
Department of Radiology
University of California, Los Angeles (UCLA) Medical School
Los Angeles, CA 90095

[4]Instiute for Biomedical Engineering, Science and Technology
The University of Oklahoma
Norman, OK 73019, USA

[*]Equal 1st-Authored Contribution

August 22, 2018

For correspondence:
Chung-Hao Lee, Ph.D.
Assistant Professor
School of Aerospace and Mechanical Engineering
Affiliated Faculty Member
Institute for Biomedical Engineering, Science, and Technology
The University of Oklahoma
865 Asp Ave., Felgar Hall Rm. 219C
Norman OK 73019-3609
email: ch.lee@ou.edu
Tel: 405-325-4842

Abstract

Intracranial aneurysms (ICAs) are focal dilations in the brain's arteries. When left untreated, ICAs can grow to the point of rupture, accounting for 50-80% of subarachnoid hemorrhage cases. Current treatments include surgical clipping and endovascular coil embolization to block circulation into the aneurysmal space for preventing aneurysm rupture. As for endovascular embolization, patients could experience aneurysm recurrence due to an incomplete coil filling or compaction over time. The use of shape memory polymers (SMPs) in place of conventional platinum coils could provide more control and predictability for mitigating these complications. This study was focused on characterization of an aliphatic urethane-based SMP to evaluate its potential as a novel biomaterial for endovascular embolization. Twelve compositions of the SMP were synthesized and their thermomechanical properties together with the shape recovery behavior were comprehensively investigated. Our results showed that the SMPs experienced a significant decrease in storage and loss moduli as heated above their glass transition temperatures (32.3°C-83.2°C), and that all SMPs were thermally stable up to 265°C. Moreover, the SMPs exhibited both composition-dependent stress relaxation and a decrease in elastic modulus during cyclic loading. The shape recovery time was less than 11 seconds for all SMP compositions, which is sufficiently short for shape changing during embolization procedures. Several candidate compositions were identified, which possess a glass transition temperature above body temperature (37°C) and below the threshold of causing tissue damage (45°C). They also exhibit high material strength and low stress relaxation behavior, suggesting their potential applicability to endovascular embolization of ICAs.

Keywords: Shape memory polymers; polyurethane; glass transition temperature; thermo-mechanical properties; endovascular embolization

1. Introduction

An intracranial aneurysm (ICA), or a cerebral aneurysm, is an abnormal focal dilation and weakening of an arterial blood vessel in the brain with a prevalence of 0.5%-6% in adults (Rinkel et al., 1998; Schievink, 1997). Although most aneurysms are asymptomatic and do not rupture, they can grow unpredictably, and even small aneurysms (size ≤ 5.0 mm) carry a risk of rupture. Incidental rupture of an ICA is most common between age 40 and 65, associated with 50%-80% of the subarachnoid hemorrhage (SAH) cases, which causes individual's death before receiving medical attention associated with a mortality rate as high as 40% within the first week, and accounts for about 5%-8% of all strokes, (Bederson et al., 2009; Connolly et al., 2012; King Jr, 1997; Lantigua et al., 2015; Naval et al., 2012; Sacco et al., 1984; Wardlaw and White, 2000).

Currently, surgical clipping and endovascular coil embolization are the two most common treatment methods for intracranial aneurysms. Clipping of intracranial aneurysms requires craniotomy and neurosurgeon places a clip across the neck of the treated aneurysm to block it from the normal circulation (Molyneux et al., 2005). In contrast, micro-catheter delivery-based endovascular therapy with Guglielmi detachable coils (GDC) (Guglielmi et al., 1991; Molyneux and Group, 2002; Raymond et al., 2003) is a minimally invasive surgical technique, which aims at excluding the aneurysmal sac and neck from intracranial circulation by means of complete and lasting occlusion. Although GDC-based coil embolization therapy has been considered as an alternative to surgical clip ligation that is associated with higher procedural mortality (Campi et al., 2007; Molyneux et al., 2009; Taha et al., 2006), recent studies (Hope et al., 1999; Tateshima et al., 2000; Vallée et al., 2003; Wehman et al., 2006) have shown that unsatisfying rates of aneurysmal recanalization and incomplete occlusion are still emerging challenges in endovascular coil embolization. Therefore, development of novel biomedical devices for the use in minimally invasive surgical procedures as tailored to patient's complex aneurysm geometry is essential to improve the long-term therapeutic outcomes of current endovascular techniques and to overcome the above-mentioned clinical challenges.

As the first logical step towards the attainment of this research objective, we, in this study, comprehensively characterize the thermomechanical properties and the shape recovery capability of aliphatic urethane shape memory polymers (SMPs) and investigate its potential applications to manufacturing individualized embolic devices for treating intracranial aneurysms. Shape memory polymers, such as polyurethane (Gunes et al., 2008; Xu et al., 2006), have aroused great attention from scientists and engineers owing to their excellent shape memory

behavior, high biocompatibility, fast shape recovery speed, and low synthesis cost. This type of polymer is synthesized using hexamethylene diisocyanate (HDI), N,N,N0,N0-tetrakis (hydroxypropyl) ethylenediamine (HPED), and Triethanolamine (TEA), and consists of two segments at the molecular level: (1) the rigid and glassy segments determining the permanent shape and (2) the amorphous segments controlling the temporary shape. Currently, most of the biocompatible SMPs used for biomedical applications are thermally induced. When heated above its glass transition temperature (T_g), the amorphous segments of the SMP transition from a glassy state to a rubbery state, allowing the polymer to deform under an external load (Huang et al., 2012). After cooling below T_g and subsequent releasing of the external loading, the temporary shape is obtained. The polymer can autonomously return to this programmed shape without external mechanical stimuli when polymer temperature increases above T_g again.

Biomedical devices fabricated using SMPs can potentially be introduced into a patient's body in a temporary, compressed shape and then be expanded on demand to their programmed shape as required. Since the shape recovery can be facilitated with a certain triggering mechanism, such as increasing temperature, the release of medical devices can be completed without additional complex surgical operations, but rather through the micro-catheter. Many biomedical devices and applications have been developed for SMPs that allow triggered responses, including self-tightened biodegradable sutures (Lendlein and Langer, 2002), a micro-actuator for blood removal (Maitland et al., 2002), and stents (Wache et al., 2003).

In this study, we aim to develop a detailed experimental procedure for the synthesis of aliphatic urethane based SMPs and perform comprehensive thermomechanical characterization on a range of SMP compositions to investigate connections between the working temperature of the polymers and their mechanical behavior. Specifically, we identify the glass transition temperatures of each composition using both dynamic mechanical analysis (DMA) and differential scanning calorimetry (DSC) tests, and we determine the threshold for thermal degradation of each composition using thermogravimetric analysis (TGA). We also report the results of uniaxial cyclic and failure testing and analyze the differences in behavior between different compositions. We conduct this research with the goal of eventually designing an advanced individualized endovascular embolization device using aliphatic urethane SMPs as the primary material. Consequentially, we discuss the results in terms of the desirable physical qualities such an implantable material that would need to possess.

2. Methods

2.1 Materials and SMP synthesis

In this work, (i) hexamethylene diisocyanate (HDI, ≥99.0%), (ii) N,N,N0,N0-tetrakis (hydroxypropyl) ethylenediamine (HPED, ≥98.0%), and (iii) Triethanolamine (TEA, ≥99.0%) were purchased from Sigma-Aldrich. All the above materials were used as received for synthesizing aliphatic urethane shape memory polymers. Twelve combinations of these three monomers were synthesized, with their respective SMP formulations given in **Table 1**.

2.2 SMP synthesis procedure

Various SMPs were synthesized by mixing different ratios of HPED, TEA, and HDI. The molar ratios for each batch were sourced from the previous study by Wilson et al. (Wilson et al., 2007) with modifications to the second and last compositions (**Table 1**). All measurement and mixing procedures occurred within a nitrogen-filled glovebox to avoid moisture contamination of the monomers (**Fig. 1a**). The glovebox received a steady flow of nitrogen through an inlet at the top of the rear panel and vented gas into a fume hood from an outlet at the bottom of the rear panel. This prevented air from entering the work space and removed any undesired moisture prior to the synthesis. Nitrogen flow could be redirected to the vacuum oven used later during synthesis via a set of ball valves.

Monomer weighing was performed using a Fisherbrand motorized pipette filler (Thermo Fisher Scientific) and a digital scale (AWS-100, American Weigh Scales). In brief, the HPED and TEA were measured in the same 100 mL glass beaker, while HDI was kept in a separate container until the stirring stage where it was added to the mixture and stirred on a magnetic stirring plate (**Fig. 1b**). The mixture was stirred gently to avoid the introduction of gas bubbles into the liquid. Stirring continued until the mixture showed a sudden transition from translucent to uniformly clear. The time required to produce this transition increased as the ratio of HPED in the mixture decreased and the ratio of HDI increased (**Table 1**).

The procedures in Wilson et al. (Wilson et al., 2007) suggested including an excess of 1-2% isocyanate (HDI). However, our early synthesis results were unsatisfactory, and the removal of this excess improved the success rate of our syntheses. We also observed a tendency of the mixtures to cure before degassing could take place, leaving large air bubbles in the resulting specimens. Since the mixture of the monomers is an exothermic reaction, we noticed large batches of the mixture could generate adequate heat to act as a catalyst for the curing process. To avoid these scenarios, we limited the size of each batch to 16g-18g, and

mixed multiple small batches during a single synthesis procedure, rather than mixing the full volume all at once.

Once the mixture had sufficiently reacted, we quickly removed it from the glovebox and poured the contents into a set of silicone rubber molds—rectangular beams (45mm x 8mm x 1mm) for glass transition-related characterizations and ASTM D638 Type V dog bones for tensile mechanical testing (c.f. **Sections 2.3 and 2.4**, respectively). Prior to the synthesis, two coats of mold release (Buehler 208186032) were applied to each specimen mold to minimize bubble generations due to any undesired interactions between the mixed monomers and the silicone rubber during curing. Then, specimen molds were placed in a vacuum oven (Being BOV-20) and 5 vacuuming (-0.8 bar) and nitrogen purging steps were performed to create a nitrogen protected environment in the oven before degassing. A strong vacuum (-0.925 bar) was next induced using a vacuum pump for 10-12 minutes to remove gas bubbles trapped in the mixture (**Fig. 1a-b**). For cases where multiple batches of mixture were used, we filled each mold half way with mixture and performed an initial degassing step while mixing the other batch. When the first degassing had finished, we filled the rest of the space of the molds and proceeded with the above-mentioned vacuuming-purging and degassing steps. An “overflow” section was included in our specimen molds to trap bubbles as introduced during the degassing procedure. The top few millimeters of each specimen could be polished off to leave a smooth finishing.

When curing the SMP specimens, we followed the procedure in Wilson el at. (Wilson et al., 2007) with several modifications. The specimens were kept at room temperature for one hour, then the temperature was increased at a steady rate to 130°C, where it was kept for another hour. The heating rate of temperature was proportional to the glass transition temperature (T_g) of the specimen being cured, to ensure each SMP had an equal curing time before reaching its T_g (**Table 1**). During the curing process, we observed a slow loss of vacuum potentially caused by the pressure increase associated with the heating. To maintain a consistent vacuum, we resealed the oven in intervals of an increase of 7.5°C, by reestablishing the vacuum (-0.4 bar) and quickly purging the system with nitrogen. Upon completion of the curing step, the SMP specimens were carefully removed from the molds and stored in a vacuum desiccator (Bel-Art Lab) to ensure no moisture contamination occurred before subsequent thermomechanical characterization experiments.

149 2.3 Characterization of the synthesized SMPs

150 The mechanical properties of shape memory polymers vary according to temperature,
151 especially in the range of their glass transition temperatures. To characterize these temperature-
152 dependent mechanical properties with various polymer compositions, we conducted a series of
153 thermomechanical tests, including the dynamic mechanical analysis (DMA), thermogravimetric
154 analysis (TGA), differential scanning calorimetry (DSC), and uniaxial tensile tests considering
155 failure and cyclic loading conditions, to pinpoint the glass transition temperature of the SMPs
156 and to better understand their thermally-dependent mechanical behaviors.

157 2.3.1 Dynamic mechanical analysis (DMA)

158 Dynamic mechanical analysis (TA Q800) was used to measure the mechanical properties of
159 synthesized SMPs. The SMP beam specimens were heated under a nitrogen atmosphere from
160 20°C to 120°C at a heating rate of 5°C/min and in the tension mode with a cyclic frequency of 1
161 Hz. DMA studies revealed the significant mechanical and thermal properties of the samples,
162 such as storage modulus, loss modulus and glass transition temperature.

163 2.3.2 Thermogravimetric analysis (TGA) and differential scanning calorimetry (DSC)

164 Thermal analysis data were measured by both thermogravimetry (TA Q50, TA Instruments)
165 and differential scanning calorimetry (TA Q20, TA Instruments). All measurements were
166 performed under nitrogen environment. In brief, the thermal degradation behavior of the samples
167 was recorded with heating from room temperature to 600°C at a rate of 10°C/min. An in-house
168 MATLAB (MathWorks) program was used to determine the onset temperature of thermal
169 degradation, which was used as reference for the ensuing DSC measurements. The program
170 performed a linear regression on a section of each specimen's TGA curve below T_g, and another
171 linear regression of the region on the TGA curve between 90% and 85% mass. The intersection
172 of these two lines was determined to be the threshold of thermal stability. DSC measurements
173 were carried out by: (1) heating from 20°C to 160°C at a rate of 5°C/min, (2) cooling to 20°C at
174 50°C/min, (3) maintaining for 3 min at 20°C, and then (4) repeating the above procedures. DSC
175 studies revealed the significant thermal properties of the samples, such as the glass transition
176 temperature. All the DSC data presented in this study were from the second heating cycle.

177 2.4 Mechanical testing for the synthesized SMPs

178 Before performing tensile and cyclic testing on the SMP dog-bone specimens, the overflow
179 region was removed to produce a clean finish on both sides of the specimen and eliminate

imperfections. The samples were polished using a custom designed and 3D printed mount on a rotary polishing machine (LaboPol-5, Struers). Once polished, the width and thickness of the testing region were measured thrice each and averaged. Tensile failure testing was conducted using a uniaxial tensile testing system (Instron 5969, Instron). Double-sided padded tape was applied to both sides of each gripping region before mounting to prevent slippage during testing.

Failure testing was conducted at 10°C above the T_g of each specimen in a temperature regulated environment on the Instron. The specimens were mounted in three steps. First, the base of the sample was clamped into the bottom set of grips and allowed to heat up to the temperature of the testing environment. Second, the top section was clamped into the top set of grips, and the distance between the two grips was measured with a caliper. After measuring the distance between the grips, the extension reading on the Instron was zeroed, and as the sample returned to testing temperature the grip positions were adjusted to keep the measured load as close to zero as possible. Finally, both sets of grips were tightened to make up for the relaxation of the SMP past its T_g. Once the sample reached testing temperature and the measured load was returned to zero, the extension measured by the Instron testing machine was added to the previously measured length and the extension was zeroed once again. This value was recorded as the initial length of the specimen. Upon starting the test, the specimens were subjected to a displacement of 2 mm/min until failure. Five failure tests were completed per specimen, and the best three were selected for characterization purposes based on relative consistency of the elastic modulus and failure stress values.

The procedures for cyclic testing closely resembled those for failure testing. Another set of dog-bone specimens were tested at 10°C above T_g and the same three step mounting procedures were exercised as previously mentioned. For the cyclic tests, each sample underwent three cycles of preconditioning at 25% of the failure strain as determined during failure testing. After the preconditioning step, the samples underwent ten loading and unloading cycles of the previously determined 50% failure strain. Both preconditioning and cycling steps were carried out at the same strain rate of 2 mm/min as the failure tests.

2.5 Quantification of shape recovery capability

The shape recovery function of the synthesized SMPs was investigated by bending a straight beam sample at a 180^0 angle, then measuring the time required for full recovery at various temperatures. We followed a method similar to the recovery tests employed by Lin et al. and Lan et al. (Lan et al., 2009; Lin and Chen, 1998a, b). In brief, the initial bend was achieved using

a 3D printed mold. The beam was heated above its glass transition temperature, and then placed into the mold where the specimen could cool and maintain its shape at the desired angle. To measure the recovery time, a video camera was placed directly above a beaker of water on a hot plate. The bent sample was held with forceps on a ring stand and swiftly lowered into the heated water bath, where the SMP specimen was fully recovered. The video was analyzed frame by frame to determine the elapsed time between any two specific angles of 45, 90, 135, 165, and 180 degrees. This procedure was conducted using water baths at T_g, T_g+5°C, and T_g+10°C for each sample. Three repeated recovery tests were conducted at each of the above temperature levels, resulting in a total of 9 recovery time measurements for each SMP composition.

3. Results

3.1 DMA results

All SMP compositions showed a single steep transition in their shear storage modulus, each occurring at a different temperature threshold (**Fig. 2a**). A tan(δ) plot (**Fig. 2b**) was used to determine the glass transition temperature of each SMP composition. These values were taken at the peak of the tan(δ) plot and decreased monotonically from SMP1 to SMP12, ranging from 83.2°C to 32.3°C (**Table 2**). The storage moduli generally increased from SMP1 to SMP12; however, SMP10 exhibited exceptionally large values both above and below its glass transition temperature. Another factor which varied with the SMP composition was the change in the storage modulus from T_g-5°C to T_g+15°C. With a few exceptions, the storage modulus of each specimen was reduced by a factor of 20-30 times its value at T_g-5°C when raised to T_g+15°C. Shear modulus values at both temperatures tended to be larger for specimens nearer to SMP12, but there was not a consistent increase from one composition to another. A notable outlier is the shear modulus of SMP10 at T_g+15°C, which is exceptionally large compared to the other compositions.

3.2 TGA results

The TGA testing results (**Fig. 3**) show two major slopes occurring near 300°C and 400°C. The distinction between these two slopes becomes more pronounced for SMP compositions closer to SMP12 that contain high percentages of the TEA. Values for the onset of thermal degradation were determined for each composition with values, showing no consistent trend, ranging from 268.2°C to 284.7°C (**Table 2**). We determined the temperature at which each SMP composition degraded to 90% of its original weight. This value varied little between specimens,

ranging from 275°C to 293°C (**Table 2**). Generally, this value increased from SMP1 to SMP12, but with an appreciable variation between individual compositions. The temperature required to degrade the SMPs to 50% weight varied more than the values for 90% degradation, ranging from 356.6^0C to 316.5^0C; however, these values showed a more uniform increase from SMP1 to SMP12 (**Table 2**).

3.3 DSC results

The results of the DSC tests were used as a secondary means of determining the T_g of each SMP composition (**Fig. 4** and **Table 2**). To extract these values, we used the local minimum of the resulting heat flow plots (**Fig. 4**), showing a monotonic decrease from SMP1 to SMP12. Such a monotonic decrease is also reflected in the T_g of the SMP compositions, ranging from 87°C to 33°C. These T_g values from the DSC testing generally agree with the values determined using the tan(δ) plot in the DMA tests (**Fig. 2**). However, the T_g values determined using DSC analysis are consistently higher than those from DMA and tan(δ) analysis, but the difference is small enough to attribute to differences arising from the method of determination. The same difference was observed in the analysis performed by Wilson et al. (Wilson et al., 2007).

3.4 Uniaxial tensile testing results

Under uniaxial tensile failure tests, the SMPs exhibited a sharp decrease in the failure stress and the failure strain from SMP1 to SMP3 and an increase in both failure stress and failure strain from SMP3 to SMP12 (**Fig. 5** and **Table 3**). The trends in the data are nonlinear, with large increases near compositions SMP12 and SMP1 (**Fig. 5**). The maximum failure stress and strain occur at SMP12 with values of 6.88 MPa ± 0.29 MPa and 54.4% ± 2.97%, respectively. The minimum stress and strain occur at SMP3 with values of 3.34 MPa ± 0.16 MPa and 16.2% ± 0.72%, respectively. For most of the specimens, we observed a decrease in both failure stress and strain as the HPED content increased in the SMP composition.

As for the uniaxial tensile cyclic tests, the SMPs show a noticeable relaxation behavior under cyclic tensile testing. This can be seen in the representative specimen (**Fig. 6a**). The relaxation behavior is different depending on the specimen composition, and it generally decreases from SMP1 to SMP12. However, this decrease is not uniform and requires more data collection before any concrete trends relating to composition can be identified. Within individual specimens, the relaxation behavior followed a regular pattern (**Fig. 6a**), exhibiting large but decreasing relaxation during the first six cycles and then transitioning to uniform small relaxation during later cycles. The maximum reduction observed at the end of the tenth cycle was 26.9% ± 3.93% for

SMP1, while the minimum was observed to be 1.15% ± 0.04% for SMP9. The elastic moduli of the SMPs were also affected by the cyclic loading, decreasing sharply during the first two cycles but remaining nearly constant after the fourth (**Fig. 6c**). The elastic modulus also varies with the SMP composition, with a gradual decrease from SMP1 to SMP12. SMP1 displayed the largest elastic modulus with a value of 22.58 MPa ± 0.08 MPa, while SMP 12 displayed the smallest, with a value of 13.14 MPa ± 0.31 MPa (**Table 3**).

3.5 Shape recovery capability

The SMPs showed a consistent temperature dependence in their shape recovery behavior, an example of which is shown in **Figure 7**. Among individual specimens, the SMPs showed a slower recovery response between the initiation of the test and the first 45° of recovery, a fast, linear response between 45° and 135°, and a nonlinear deceleration as it approached a full 180° recovery. The results of the recovery tests indicated no significant trends in the recovery time with relation to the SMP composition. There was a tendency for specimens with a high TEA content (closer to SMP12) to recover faster than those with a high HPED content (closer to SMP1). However, several SMP compositions fell outside of this trend that it cannot be considered significant. **Figure 8** shows a direct comparison of the recovery test results at T_g+5°C among 3 selected SMP compositions (SMP3, SMP7, and SMP11).

4. Discussion

4.1 Overall findings and relevance to endovascular embolization treatment for ICAs

The thermomechanical characterization of the aliphatic urethane SMPs provided a closer look at the shift in material properties that occurs as each SMP reaches its T_g. The DMA results showed a single sharp transition in the shear storage modulus for all compositions (**Fig. 2a**). We observed that this transition occurs at different temperature levels depending on the SMP composition, with higher glass transition temperatures corresponding to higher concentrations of HPED. In this study, the glass transition temperature of the SMP specimen was determined from these transitions with SMP compositions tested, ranging from 83.2°C to 32.3°C. In the context of implantable embolic devices, the SMP needs to possess a T_g above body temperature (37°C) but below the threshold for tissue damage (45°C) (Wang et al., 2014). If the T_g is below body temperature, then the implant would constantly exist in a malleable state and not hold any one specific shape; however, at temperature levels greater than 45°C, bodily tissues can begin to take damage. This desired threshold falls within our observed T_g values, suggesting that we

307 can synthesize an aliphatic urethane SMP by employing the techniques detailed in this study,
308 which transitions at a temperature suitable for applications in the human body.

309 Moreover, uniaxial mechanical testing was conducted using the SMPs to determine their
310 material strength and investigate how the strengths varied with composition. The failure test
311 results suggested that higher values for both failure stress and strain occur in compositions with
312 lower HPED contents, but the trend is nonlinear with significant variances at SMP3 (**Fig. 5**).
313 Because of its irregular trends, this data will be difficult to use in a predictive manner, but it
314 implies that there may be more complex changes associated with the SMP's composition than
315 we previously expected. With a wider range of compositions and larger sample sizes for each
316 composition, future studies could identify trends which could allow fabrications of SMP-based
317 biomedical devices with specific material strengths.

318 Cyclic tensile testing was performed to investigate changes in the behavior of the SMP
319 under repeated loading. The two major properties that we investigated were the elastic modulus
320 and the peak stress value at 50% failure strain (**Table 3**). GDC-based coils are designed to be
321 left in the body for the remainder of a patient's lifetime, so it is important that the SMP materials
322 used for this endovascular embolization application will not relax over time, resulting in the
323 aneurysm recurrence. One behavior that the cyclic testing revealed was a noticeable reduction
324 in the peak stress, with most of the reduction occurring during the first few cycles. This stress
325 reduction reached a maximum value of 26.9% ± 3.93% in SMP1 with respect to the first cycle,
326 and the next highest values fell near the range of 8%-9% for SMPs 2-5. The relaxation behavior,
327 which is not a desirable quality in the context of a permanent embolization device, was more
328 pronounced for SMPs containing more HPED contents. The compositions containing large
329 quantities of TEA contents exhibited less relaxation, reaching values as low as 1.15% ± 0.04%
330 for SMP9 and 1.92% ± 1.36% for SMP11. However, due to a small sample size for our cyclic
331 tests, we were not able to identify any quantitative relationship between the SMP composition
332 and the stress relaxation behavior. In addition, the elastic modulus also varied with cyclic loading,
333 but only during the first few cycles of the test. The elastic modulus values decreased sharply
334 during the first cycle, but quickly reached a constant value around the third or fourth cycle (**Fig.**
335 **6a**). Even though the changes in elastic modulus are small, it is in our interest to minimize any
336 changes in material properties once the SMP is introduced into the body. Since we were able to
337 observe both the stress relaxation and elastic modulus approaching a stable point in the latter
338 cycles of our tests, we expect that it would be necessary to design the embolization devices to

undergo pre-cycling before implantation, minimizing the effects of initial relaxation when the device is administered.

Another important factor in designing an embolic device made from SMPs is the shape recovery behavior which occurs when the polymer transitions from a deformed state to its un-stressed state. The recovery tests conducted in this study focused on the time required for the SMP to recover its shape. For endovascular embolization of ICAs, short recovery time of the SMP-based device is an important design criterion to avoid the prolonged heating of body tissues during device deployment. We showed the recovery behavior of the SMPs to be temperature dependent, speeding up as temperatures increased past the T_g. At T_g+10°C, with no composition taking more than 10.3 seconds to fully recover from a 180° bend. There was noticeable variation among different compositions, and it is very likely that a more complex relationship exists between the SMP composition and the polymer's recovery behavior. Such relationships are beyond the scope of this study and could be further investigated in the future. The quick recovery time displayed by all compositions is promising for our continued efforts toward the development of an improved aneurysm embolization device. If a device made using this SMP material could be intravenously moved to its target location and then reconfigured in a matter of seconds, it would have the ability to improve a great number of medical procedures.

4.2 Study limitations and Future Work

This study featured a comprehensive set of thermomechanical characterization experiments, and as a result had a plethora of limiting factors that could have contributed to the variations in our data. The most prominent of these limitations is a relative smaller sample size for our cyclic tensile test, failure test, and recovery test. Two sets of data for each composition were taken during cyclic testing, and three were taken for each composition during failure testing. For the recovery tests, three trials were performed for each temperature point for each composition. The focus of this study was to conduct a broad analysis of aliphatic urethane shape memory polymers with varying SMP compositions. Consequently, we sacrificed the data statistical meaningfulness that comes with a large sample size to instead survey a wide range of compositions for trends and patterns. As future extensions based on the results of this general characterization, we plan to focus on a single composition range and collect more thorough measurements to quantitatively define the trends observed in this study.

Within the uniaxial failure and cyclic tensile tests, there are several factors that could have affected our results. The samples that we used were all synthesized at the beginning of our

testing period, and so it is possible that the ones that were tested later in the study could have changed over time as they were stored (e.g., absorbing moisture). This could be remedied by testing each composition at the same amount of time after synthesis to ensure age is constant. The sample were attached to the uniaxial tester using double sided tape to avoid slippage. Deformations in this tape layer or slight slippages on the adhesive could have resulted in skewed results. However, since all samples were tested the same way, the error due to this mounting method should be consistent. Small imperfections in the samples, such as bubbles or heterogeneity in the monomer mixtures, could have also resulted in differences between samples in a composition. These errors can be reduced as the synthesis procedure is perfected, and researchers should be careful to select only pristine samples for testing.

The recovery tests we conducted had many aspects that can be improved upon. Our measurement method relied on visual inspection to determine the angular position of the sample and the frame at which the position of interest was reached. From the frame analysis, we determined time elapsed. This entire measurement method is subject to human error in multiple places, which is difficult to account for. It would be beneficial to determine a more exact way to measure recovery. Some samples did not return completely to a straight angle, and others began their deformation at an angle other than 180^0. While the recovery times were still useful for our analyses, a study looking to definitively quantify the recovery response of these materials would need to better define the start and end conditions for the tests.

It is essential that endovascular devices are visible under x-ray based fluoroscopy so that physicians can pinpoint their location and orientation during device deployment. Urethane-based shape memory polymers are typically invisible to radiographic imaging techniques, and, therefore, the addition of radio-opaque additives to the polymer composition is necessary for their use in the endovascular embolization applications. For instance, Wong et al. created composite blends of poly (DL-lactide-co-glycolide) (PLGA) with both tantalum and bismuth (III) oxychloride, which appeared clearly in radiographic images whereas the shape memory effect can be maintained (Wong et al., 2016). While not investigated in this study, we plan to examine different radio-opaque additives in our aliphatic urethane SMP and determine any resulting changes in the SMP material properties.

The use of heat as an activation mechanism of SMP shape recovery poses many challenges, especially in an area as sensitive as the brain artery vessel tissues. Although our study has identified a range of SMP compositions that transition at biologically safe temperatures,

the challenge of delivering the thermal stimulus remains. There is a wealth of literature discussing diverse activation techniques, many of which are based on the indirect delivery of thermal energy to the material. These methods include, but are not limited to, Joule heating with the addition of conductive inclusions, optical heating achieved using wavelength specific dyes and a matching laser light source, and magnetic stimulation of nanoparticles (Huang et al., 2013; Small et al., 2007). Another activation technique uses chemical interactions to lower the T_g of the SMP below ambient temperature, triggering the shape memory effect. This effect occurs slowly in polyurethane SMPs, and quickly in hydrogels, when the materials are exposed to water (Huang et al., 2005; Lu and Du, 2014; Salvekar et al., 2017; Wong et al., 2016). As part of our future extensions, we plan to test a wide range of activation techniques to determine the method most suitable for the deployment of an endovascular embolization device. Because of the slow reaction to water that has been observed in polyurethane SMPs from the research of Huang et al. and Lu et al., we also intend to study the long-term effects of moisture on our embolic devices after deployment (Huang et al., 2005; Lu et al., 2014).

4.3 Conclusion

This study aimed to characterize a range of compositions of aliphatic urethane shape memory polymers for their potential use in the treatment of intracranial aneurysms. In specific, we developed a detailed synthesis procedure for the SMPs to provide our study with a variety of compositions and inform future studies seeking to utilize the same material. We have investigated the thermomechanical properties including the glass transition temperature and thermal stability of each composition, and we have also found that compositions between SMP9 and SMP11 possess transition temperatures between body temperature and the threshold of tissue damage. This is the optimal T_g range for allowing the polymers to remain functionable within the body without causing any tissue damage due to the heating associated with shape change triggering. We have also found that within our desired operating temperatures, all SMP compositions are thermally stable regarding the endovascular embolization procedure. We have also characterized the mechanical properties of the SMPs and identified decreases in both maximum stress and elastic modulus with cyclic loading. Our results showed that in SMPs closer to SMP12, these decreases were not as prominent. Since any changes in material properties during the lifetime of an implanted device are detrimental, the SMP compositions near SMP12 are more desirable in the context of endovascular embolization treatment for ICAs. Finally, we have tested the recovery time of each polymer and showed that all the SMP compositions are

capable of recovering from a 180° bend within 10.3 seconds. Using knowledge from the broad characterization performed in this study, we have identified a range of compositions between SMP9 and SMP11 that most accurately meet our criteria with their great potential for the individualized treatment of intracranial aneurysms, and they will be analyzed further in more detail as a part of future studies.

Acknowledgments

Funding support from the Oklahoma Shared Clinical and Translational Resources (OSCTR) Pilot Project Program (NIGMS U54GM104938) and the Oklahoma Center for the Advancement of Science & Technology (OCAST) Health Research Program is gratefully acknowledged. CHL was in part supported by the institutional start-up funds from the School of Aerospace and Mechanical Engineering (AME) and the research funding through the SEED Funding for Interdisciplinary Research from the Gallogly College of Engineering and the Faculty Investment Program from the Research Council at the University of Oklahoma (OU). RK and DL were supported by the Mentored Research Fellowship from the Office of Undergraduate Research at OU.

Conflicts of Interest

None of the authors have a conflict of interest with the present work.

Tables

Table 1. Percent monomer content, monomer-mixture stirring time, and the curing heating rate for all the twelve SMP compositions.

	Monomer Content (%)			Stirring Time (seconds)	Heating Rate (°C/hour)
	HDI	HPED	TEA		
SMP1	53.5	46.5	0.0	150	30.0*
SMP2	53.9	44.5	1.6	170	29.6
SMP3	54.3	42.5	3.2	200	29.2
SMP4	55.1	38.4	6.5	225	26.4
SMP5	56.0	34.1	9.9	240	25.2
SMP6	56.9	29.7	13.4	255	23.6
SMP7	57.8	25.1	17.1	270	21.1
SMP8	58.8	20.4	20.8	285	18.5
SMP9	59.7	15.6	24.7	310	15.9
SMP10	60.7	10.6	28.7	330	12.5
SMP11	61.8	5.4	32.8	350	9.6
SMP12	62.3	2.7	35.0	445	8.5

*Suggested same heating rate for SMP curing in Wilson et al. (Wilson et al., 2007).

Table 2. Glass transition temperature (T_g) and storage modulus from the DMA tests (c.f. **Fig. 2**), T_g from the DSC tests (c.f. **Fig. 4**), and the temperature levels associated with 90% and 50% remaining weights of the SMPs from the TGA tests (c.f. **Fig. 3**).

	DMA			DSC	TGA		
	T_g (°C)	Storage modulus at T_g-5°C (MPa)	Storage modulus at T_g+15°C (MPa)	T_g (°C)	Temperature (°C) associated with the onset of thermal degradation	Temperature (°C) associated with 90% remaining weight	Temperature (°C) associated with 50% remaining weight
SMP1	83.2	403.3	13.3	87	276.6	289.5	356.6
SMP2	79.5	442.0	13.4	83	278.2	288.7	353.6
SMP3	72.6	459.4	15.7	76	276.6	286.3	351.4
SMP4	65.7	529.6	19.3	73	284.7	293.5	351.0
SMP5	61.1	563.4	22.4	67	277.5	287.1	342.8
SMP6	55.5	589.8	26.8	63	276.8	285.5	341.2
SMP7	52.5	649.9	23.7	56	275.9	284.5	338.1
SMP8	47.5	759.4	46.0	53	278.4	285.8	333.8
SMP9	42.6	706.4	24.6	45	276.7	284.8	331.0
SMP10	37.2	882.7	142.7	39	270.8	279.2	321.2
SMP11	33.9	830.9	43.8	34	268.2	275.5	316.5
SMP12	32.3	867.7	23.9	33	272.8	279.3	318.7

Table 3. Failure stresses and failure strains from the uniaxial tensile failure testing (c.f. **Fig. 5**) and the stress reductions and the calculated elastic modulus from the uniaxial cyclic tensile testing (c.f. **Fig. 6**) for all the twelve SMP compositions. Tensile tests conducted at Tg+10°C.

	Uniaxial Tensile Failure Test		Uniaxial Cyclic Tensile Test		
	Failure stress (MPa)	Failure strain (%)	Cumulative stress reduction (%)		Elastic modulus at the 10th cycle (MPa)
			2nd cycle w.r.t. 1st cycle	10th cycle w.r.t. 1st cycle	
SMP1	4.68 ± 0.23	26.5 ± 2.11	7.66 ± 0.42	26.9 ± 3.93	22.58 ± 0.08
SMP2	3.78 ± 0.21	22.1 ± 1.24	3.36 ± 0.98	7.88 ± 2.16	20.74 ± 0.52
SMP3	3.34 ± 0.16	16.2 ± 0.72	1.83 ± 0.59	9.08 ± 4.58	18.97 ± 0.33
SMP4	3.84 ± 0.07	20.9 ± 0.32	3.14 ± 0.03	9.06 ± 0.54	19.84 ± 0.04
SMP5	3.74 ± 0.22	25.3 ± 0.76	3.30 ± 0.62	8.39 ± 1.66	18.80 ± 0.82
SMP6	4.11 ± 0.17	28.7 ± 0.83	2.79 ± 0.03	6.64 ± 0.49	20.39 ± 1.48
SMP7	4.29 ± 0.11	30.9 ± 3.14	2.28 ± 0.29	5.68 ± 0.37	18.50 ± 0.18
SMP8	4.45 ± 0.43	31.6 ± 2.44	2.26 ± 0.25	6.70 ± 0.24	19.04 ± 0.77
SMP9	4.76 ± 0.28	32.7 ± 0.58	0.41 ± 0.12	1.15 ± 0.04	18.34 ± 2.12
SMP10	4.74 ± 0.14	36.5 ± 2.14	0.51 ± 0.09	7.42 ± 0.03	16.32 ± 0.52
SMP11	5.25 ± 0.55	43.2 ± 6.29	0.80 ± 0.47	1.92 ± 1.36	15.26 ± 0.25
SMP12	6.88 ± 0.29	54.4 ± 2.97	0.93 ± 0.06	3.34 ± 0.85	13.14 ± 0.31

Figure Captions

Figure 1 – (a) Top-view schematic of the in-house equipment used in the shape memory polymer synthesis. (b) An illustration of the synthesis procedure showing specifically (i) the measurement of each monomer, (ii) the mixture of monomers to form the polymer, (iii) the deposition of the mixture into previously cast molds, and (iv) the curing of the mixture in a vacuum oven.

Figure 2 – (a) Shear storage modulus of all the twelve SMP compositions as directly measured from the DMA tests, and (b) tan(δ) curves as derived from the DMA testing results for determining the T_g of each SMP composition.

Figure 3 – TGA results showing the decomposition of the SMP with increasing temperature.

Figure 4 – DSC results used for determinations of the T_g for each SMP composition.

Figure 5 – Mean ± SEM of the failure stress (blue filled squares) and failure strain (red filled circles) for all the twelve SMP compositions (n=2) under uniaxial tension testing (T_g+10°C).

Figure 6 – Representative cyclic mechanical testing results (SMP3) when tested at 50% of the observed failure strain (T_g+10°C) showing: (a) the relaxation trend in the peak stress with an increasing number of cycles, (b) the increase in the cumulative stress reduction and (c) the convergence of the elastic modulus with an increasing number of cycles.

Figure 7 – Mean ± SEM of the recovery testing time for a representative SMP composition (SMP3, n=3) showing the consistent trend of reduced recovery time with an increased temperature.

Figure 8 – Representative experimental photos of the recovery testing for three representative SMP compositions (SMP3, SMP7, and SMP11) at defined time increments (t = 0 sec, t = 2 sec, t = 4 sec, and t = 6 sec), showing the observed trend of a decreasing recovery time with an increasing TEA content.

References

Bederson, J.B., Connolly, E.S., Batjer, H.H., Dacey, R.G., Dion, J.E., Diringer, M.N., Duldner, J.E., Harbaugh, R.E., Patel, A.B., Rosenwasser, R.H., 2009. Guidelines for the management of aneurysmal subarachnoid hemorrhage a statement for healthcare professionals from a special Writing Group of the Stroke Council, American Heart Association. Stroke 40, 994-1025.

Campi, A., Ramzi, N., Molyneux, A.J., Summers, P.E., Kerr, R.S., Sneade, M., Yarnold, J.A., Rischmiller, J., Byrne, J.V., 2007. Retreatment of ruptured cerebral aneurysms in patients randomized by coiling or clipping in the International Subarachnoid Aneurysm Trial (ISAT). Stroke 38, 1538-1544.

Connolly, E.S., Rabinstein, A.A., Carhuapoma, J.R., Derdeyn, C.P., Dion, J., Higashida, R.T., Hoh, B.L., Kirkness, C.J., Naidech, A.M., Ogilvy, C.S., 2012. Guidelines for the management of aneurysmal subarachnoid hemorrhage: a guideline for healthcare professionals from the American Heart Association/American Stroke Association. Stroke 43, 1711-1737.

Guglielmi, G., Viñuela, F., Dion, J., Duckwiler, G., 1991. Electrothrombosis of saccular aneurysms via endovascular approach: part 2: preliminary clinical experience. J. Neurosurg. 75, 8-14.

Gunes, I.S., Cao, F., Jana, S.C., 2008. Effect of thermal expansion on shape memory behavior of polyurethane and its nanocomposites. Journal of Polymer Science Part B: Polymer Physics 46, 1437-1449.

Hope, J.A., Byrne, J.V., Molyneux, A.J., 1999. Factors influencing successful angiographic occlusion of aneurysms treated by coil embolization. Am. J. Neuroradiol. 20, 391-399.

Huang, H.-Y.S., Balhouse, B.N., Huang, S., 2012. Application of simple biomechanical and biochemical tests to heart valve leaflets: implications for heart valve characterization and tissue engineering. Proceedings of the Institution of Mechanical Engineers, Part H: Journal of Engineering in Medicine 226, 868-876.

Huang, W., Yang, B., An, L., Li, C., Chan, Y., 2005. Water-driven programmable polyurethane shape memory polymer: demonstration and mechanism. Appl. Phys. Lett. 86, 114105.

Huang, W.M., Song, C., Fu, Y.Q., Wang, C.C., Zhao, Y., Purnawali, H., Lu, H., Tang, C., Ding, Z., Zhang, J., 2013. Shaping tissue with shape memory materials. Adv. Drug Del. Rev. 65, 515-535.

King Jr, J.T., 1997. Epidemiology of aneurysmal subarachnoid hemorrhage. Neuroimaging Clin. N. Am. 7, 659.

Lan, X., Liu, Y., Lv, H., Wang, X., Leng, J., Du, S., 2009. Fiber reinforced shape-memory polymer composite and its application in a deployable hinge. Smart Materials and Structures 18, 024002.

Lantigua, H., Ortega-Gutierrez, S., Schmidt, J.M., Lee, K., Badjatia, N., Agarwal, S., Claassen, J., Connolly, E.S., Mayer, S.A., 2015. Subarachnoid hemorrhage: who dies, and why? Critical care 19, 309.

Lendlein, A., Langer, R., 2002. Biodegradable, elastic shape-memory polymers for potential biomedical applications. Science 296, 1673-1676.

Lin, J., Chen, L., 1998a. Study on shape‐memory behavior of polyether‐based polyurethanes. I. Influence of the hard‐segment content. J. Appl. Polym. Sci. 69, 1563-1574.

Lin, J., Chen, L., 1998b. Study on shape‐memory behavior of polyether‐based polyurethanes. II. Influence of soft‐segment molecular weight. J. Appl. Polym. Sci. 69, 1575-1586.

Lu, H., Du, S., 2014. A phenomenological thermodynamic model for the chemo-responsive shape memory effect in polymers based on Flory–Huggins solution theory. Polymer Chemistry 5, 1155-1162.

Lu, H., Huang, W.M., Fu, Y.Q., Leng, J., 2014. Quantitative separation of the influence of hydrogen bonding of ethanol/water mixture on the shape recovery behavior of polyurethane shape memory polymer. Smart Materials and Structures 23, 125041.

Maitland, D.J., Metzger, M.F., Schumann, D., Lee, A., Wilson, T.S., 2002. Photothermal properties of shape memory polymer micro‐actuators for treating stroke. Lasers Surg. Med. 30, 1-11.

Molyneux, A., Group, I.S.A.T.C., 2002. International Subarachnoid Aneurysm Trial (ISAT) of neurosurgical clipping versus endovascular coiling in 2143 patients with ruptured intracranial aneurysms: a randomised trial. Lancet 360, 1267-1274.

Molyneux, A.J., Kerr, R.S., Birks, J., Ramzi, N., Yarnold, J., Sneade, M., Rischmiller, J., collaborators, I., 2009. Risk of recurrent subarachnoid haemorrhage, death, or dependence and standardised mortality ratios after clipping or coiling of an intracranial aneurysm in the International Subarachnoid Aneurysm Trial (ISAT): long-term follow-up. The Lancet Neurology 8, 427-433.

Molyneux, A.J., Kerr, R.S., Yu, L.-M., Clarke, M., Sneade, M., Yarnold, J.A., Sandercock, P., Group, I.S.A.T.C., 2005. International subarachnoid aneurysm trial (ISAT) of neurosurgical clipping versus endovascular coiling in 2143 patients with ruptured intracranial aneurysms: a randomised comparison of effects on survival, dependency, seizures, rebleeding, subgroups, and aneurysm occlusion. The Lancet 366, 809-817.

Naval, N.S., Chang, T., Caserta, F., Kowalski, R.G., Carhuapoma, J.R., Tamargo, R.J., 2012. Impact of pattern of admission on outcomes after aneurysmal subarachnoid hemorrhage. J. Crit. Care 27, 532. e531-532. e537.

Raymond, J., Guilbert, F., Weill, A., Georganos, S.A., Juravsky, L., Lambert, A., Lamoureux, J., Chagnon, M., Roy, D., 2003. Long-term angiographic recurrences after selective endovascular treatment of aneurysms with detachable coils. Stroke 34, 1398-1403.

Rinkel, G.J., Djibuti, M., Algra, A., Van Gijn, J., 1998. Prevalence and risk of rupture of intracranial aneurysms. Stroke 29, 251-256.

Sacco, R.L., Wolf, P.A., Bharucha, N.E., Meeks, S.L., Kannel, W.B., Charette, L.J., McNamara, P.M., Palmer, E.P., D'Agostino, R., 1984. Subarachnoid and intracerebral hemorrhage Natural history, prognosis, and precursive factors in the Framingham Study. Neurology 34, 847-847.

Salvekar, A.V., Huang, W.M., Xiao, R., Wong, Y.S., Venkatraman, S.S., Tay, K.H., Shen, Z.X., 2017. Water-responsive shape recovery induced buckling in biodegradable photo-cross-linked poly (ethylene glycol)(PEG) hydrogel. Acc. Chem. Res. 50, 141-150.

Schievink, W.I., 1997. Intracranial aneurysms. New Engl. J. Med. 336, 28-40.

Small, W., Buckley, P.R., Wilson, T.S., Benett, W.J., Hartman, J., Saloner, D., Maitland, D.J., 2007. Shape memory polymer stent with expandable foam: a new concept for endovascular embolization of fusiform aneurysms. IEEE Trans. Biomed. Eng. 54, 1157-1160.

Taha, M.M., Nakahara, I., Higashi, T., Iwamuro, Y., Iwaasa, M., Watanabe, Y., Tsunetoshi, K., Munemitsu, T., 2006. Endovascular embolization vs surgical clipping in treatment of cerebral aneurysms: morbidity and mortality with short-term outcome. Surg. Neurol. 66, 277-284.

Tateshima, S., Murayama, Y., Gobin, Y.P., Duckwiler, G.R., Guglielmi, G., Viñuela, F., 2000. Endovascular treatment of basilar tip aneurysms using Guglielmi detachable coils: anatomic and clinical outcomes in 73 patients from a single institution. Neurosurgery 47, 1332-1342.

Vallée, J.-N., Aymard, A., Vicaut, E., Reis, M., Merland, J.-J., 2003. Endovascular Treatment of Basilar Tip Aneurysms With Guglielmi Detachable Coils: Predictors of Immediate and Long-term Results with Multivariate Analysis—6-year Experience. Radiology 226, 867-879.

Wache, H., Tartakowska, D., Hentrich, A., Wagner, M., 2003. Development of a polymer stent with shape memory effect as a drug delivery system. J. Mater. Sci. Mater. Med. 14, 109-112.

Wang, H., Wang, B., Normoyle, K.P., Jackson, K., Spitler, K., Sharrock, M.F., Miller, C.M., Best, C., Llano, D., Du, R., 2014. Brain temperature and its fundamental properties: a review for clinical neuroscientists. Front. Neurosci. 8, 307.

Wardlaw, J., White, P., 2000. The detection and management of unruptured intracranial aneurysms. Brain 123, 205-221.

Wehman, J.C., Hanel, R.A., Levy, E.I., Hopkins, L.N., 2006. Giant cerebral aneurysms: endovascular challenges. Neurosurgery 59, S3-125.

Wilson, T., Bearinger, J., Herberg, J., Marion, J., Wright, W., Evans, C., Maitland, D., 2007. Shape memory polymers based on uniform aliphatic urethane networks. J. Appl. Polym. Sci. 106, 540-551.

Wong, Y.S., Salvekar, A.V., Da Zhuang, K., Liu, H., Birch, W.R., Tay, K.H., Huang, W.M., Venkatraman, S.S., 2016. Bioabsorbable radiopaque water-responsive shape memory embolization plug for temporary vascular occlusion. Biomaterials 102, 98-106.

Xu, J., Shi, W., Pang, W., 2006. Synthesis and shape memory effects of Si–O–Si cross-linked hybrid polyurethanes. Polymer 47, 457-465.

(a)

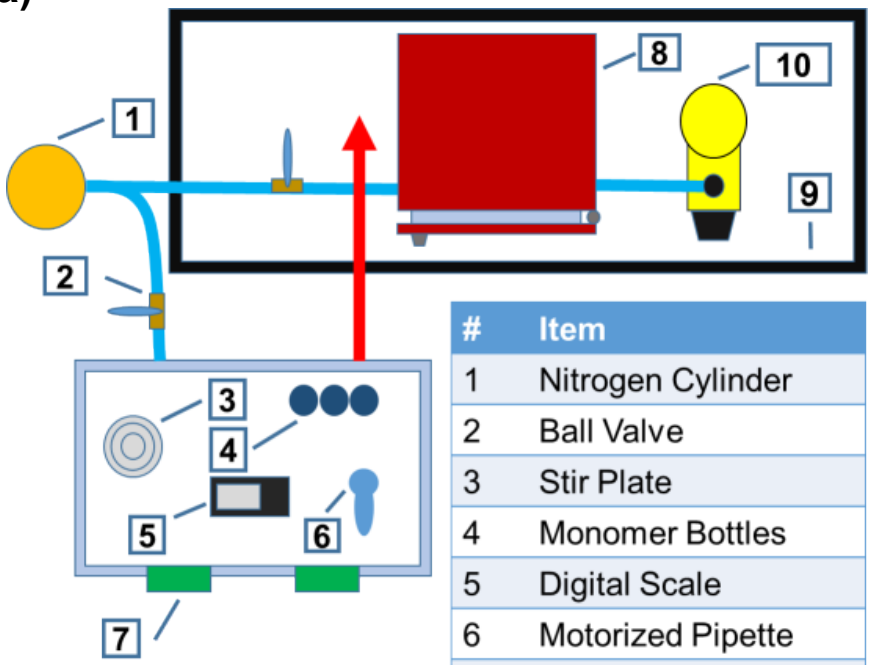

#	Item
1	Nitrogen Cylinder
2	Ball Valve
3	Stir Plate
4	Monomer Bottles
5	Digital Scale
6	Motorized Pipette
7	Glove Ports
8	Vacuum Oven
9	Fume Hood
10	Vacuum Pump

(b)

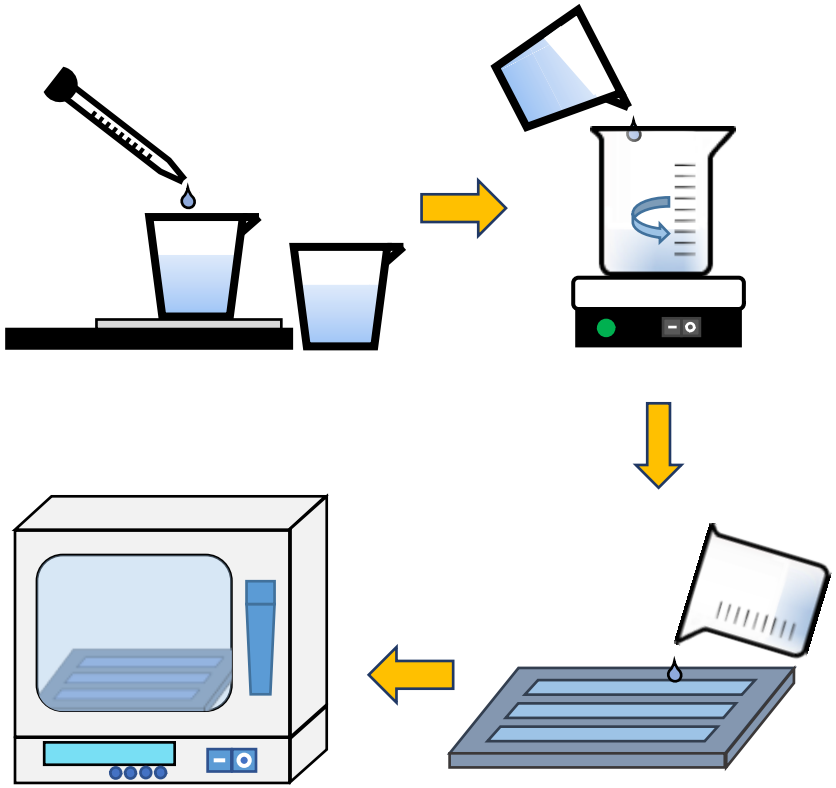

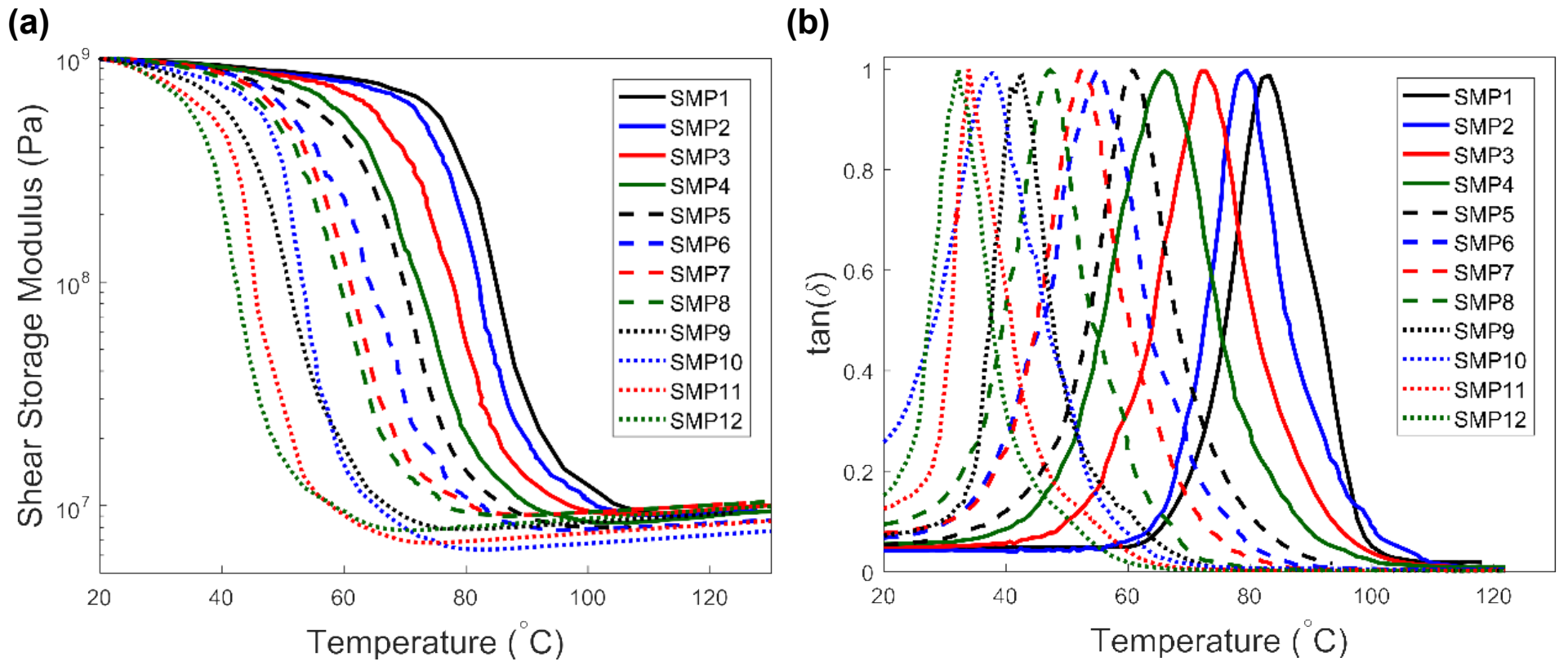
(a)
Shear Storage Modulus (Pa)
10^9
10^8
10^7
20
40
60
80
100
120
Temperature (°C)
SMP1
SMP2
SMP3
SMP4
SMP5
SMP6
SMP7
SMP8
SMP9
SMP10
SMP11
SMP12
(b)
tan(δ)
0
0.2
0.4
0.6
0.8
1
20
40
60
80
100
120
Temperature (°C)
SMP1
SMP2
SMP3
SMP4
SMP5
SMP6
SMP7
SMP8
SMP9
SMP10
SMP11
SMP12

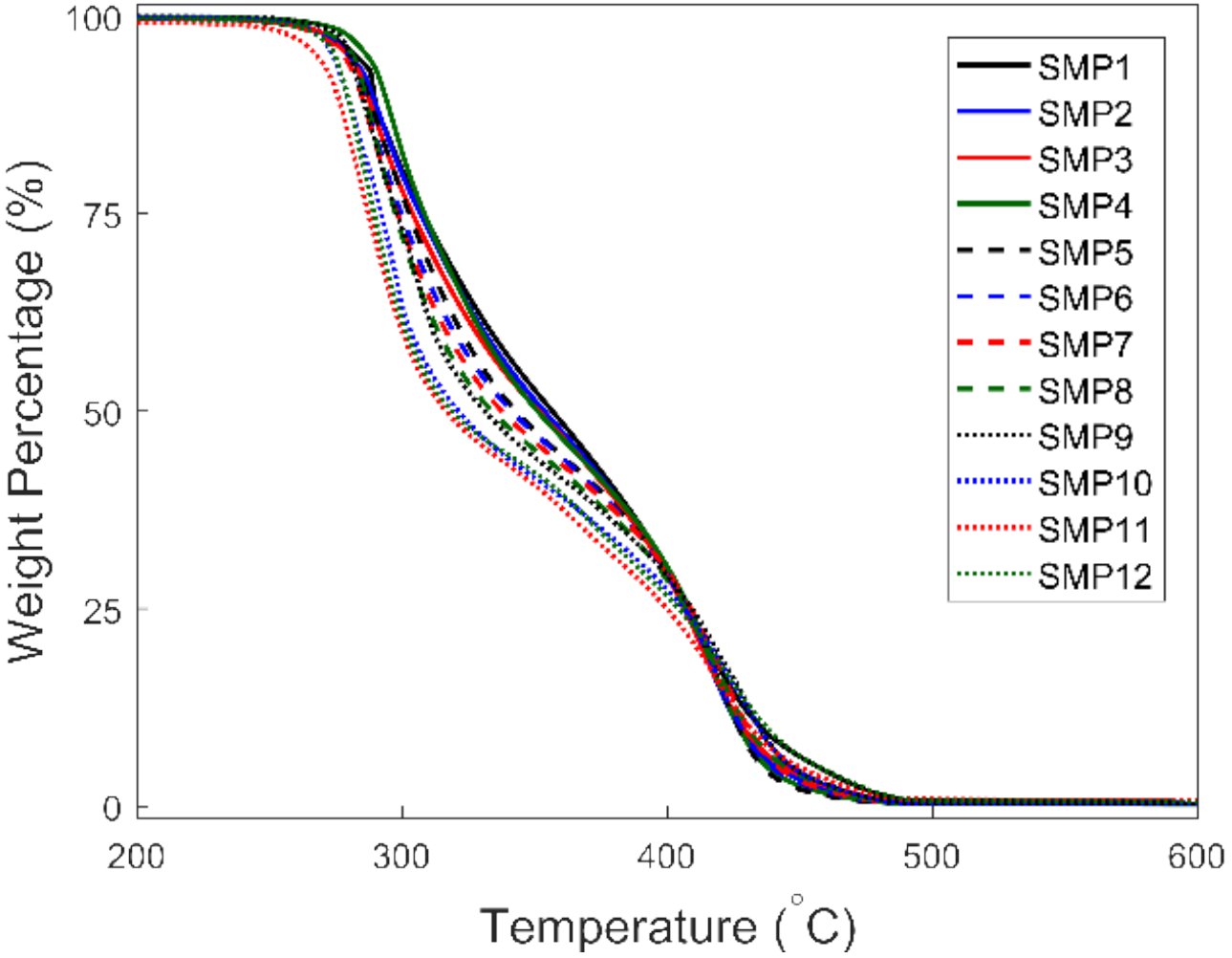
100
75
50
25
0
Weight Percentage (%)
200
300
400
500
600
Temperature (°C)
SMP1
SMP2
SMP3
SMP4
SMP5
SMP6
SMP7
SMP8
SMP9
SMP10
SMP11
SMP12

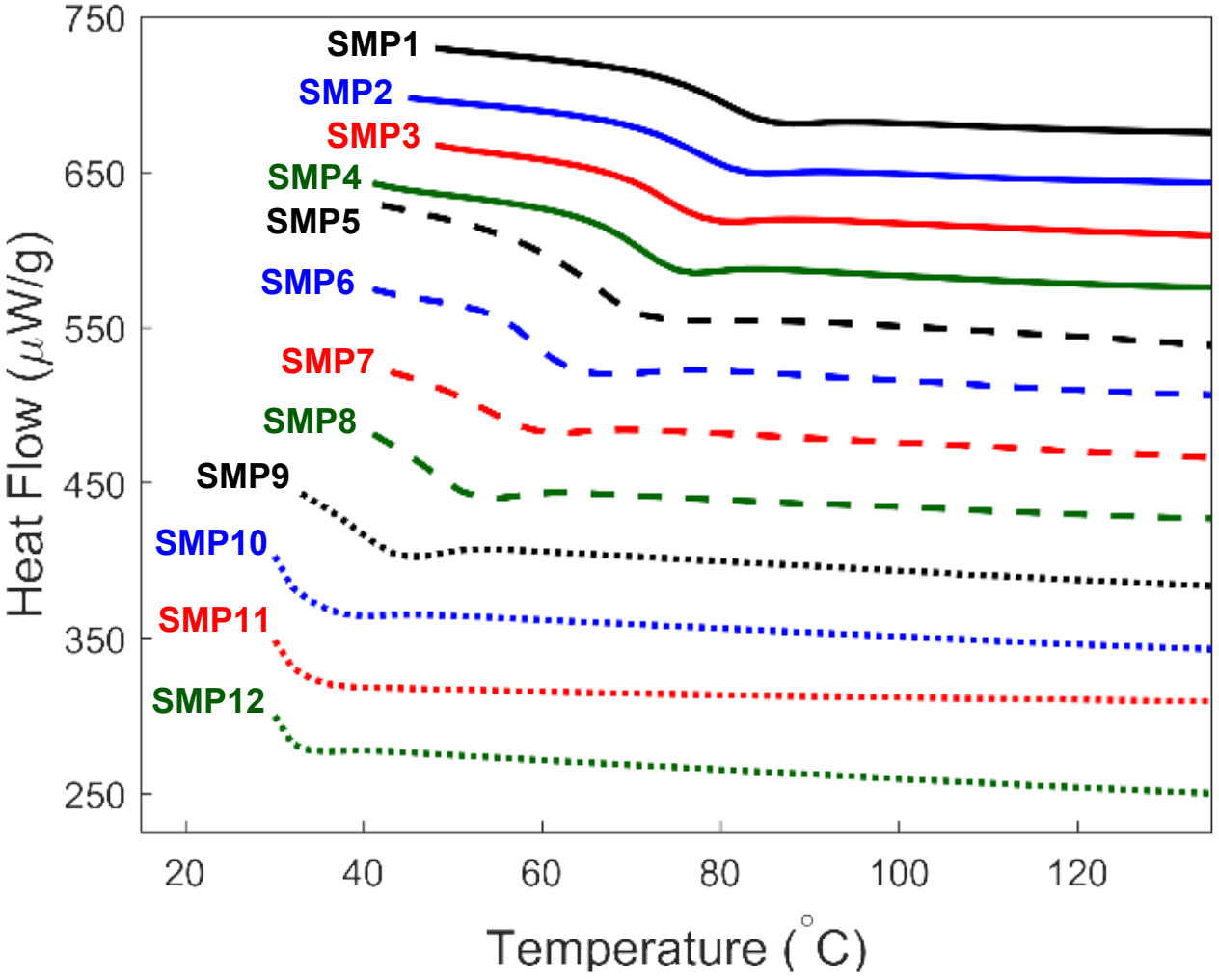
750
650
550
450
350
250
Heat Flow (μW/g)
20
40
60
80
100
120
Temperature ($^{\circ}$C)
SMP1
SMP2
SMP3
SMP4
SMP5
SMP6
SMP7
SMP8
SMP9
SMP10
SMP11
SMP12

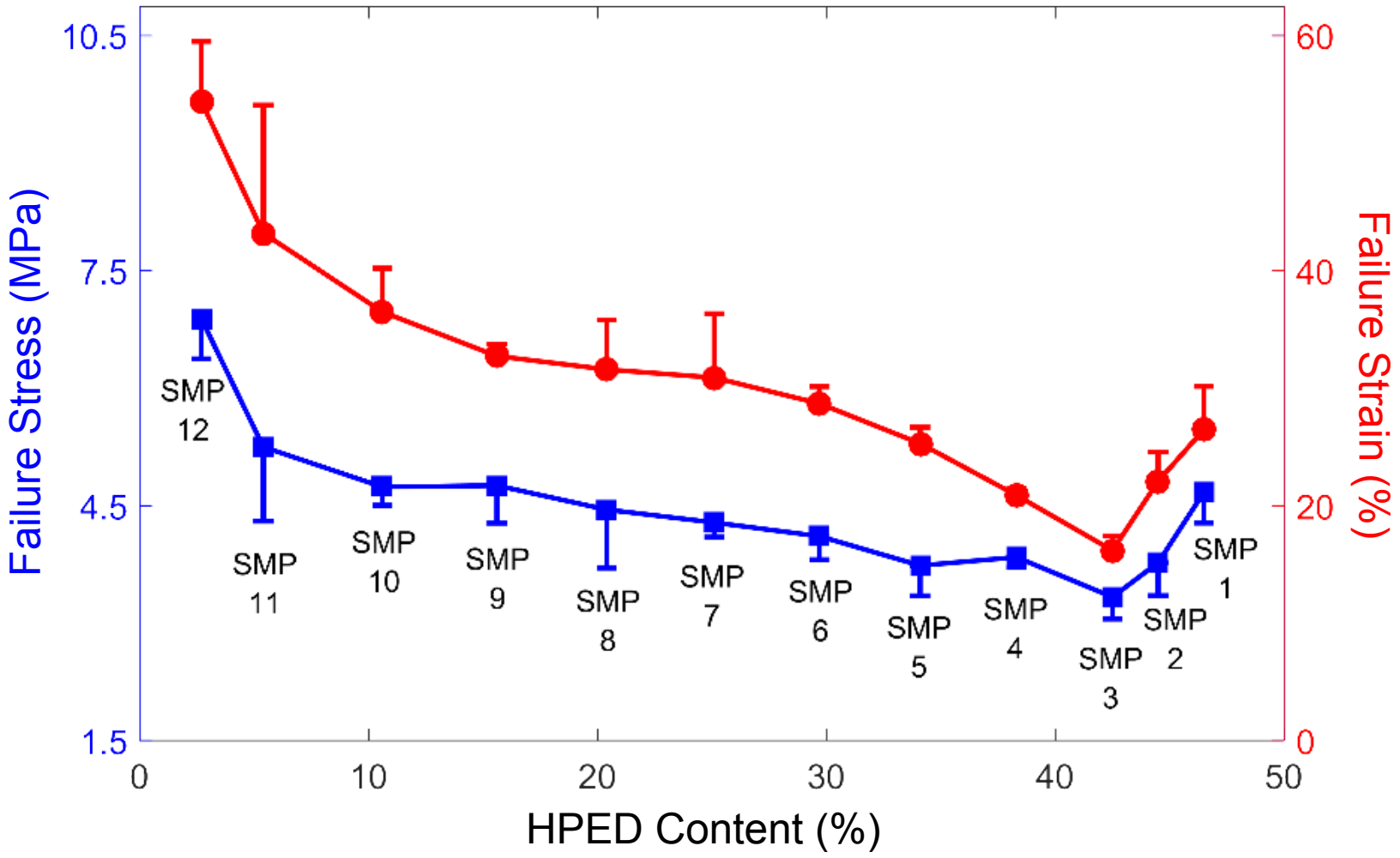
Failure Stress (MPa)
Failure Strain (%)
HPED Content (%)
10.5
7.5
4.5
1.5
60
40
20
0
0
10
20
30
40
50
SMP 12
SMP 11
SMP 10
SMP 9
SMP 8
SMP 7
SMP 6
SMP 5
SMP 4
SMP 3
SMP 2
SMP 1

Figure 6

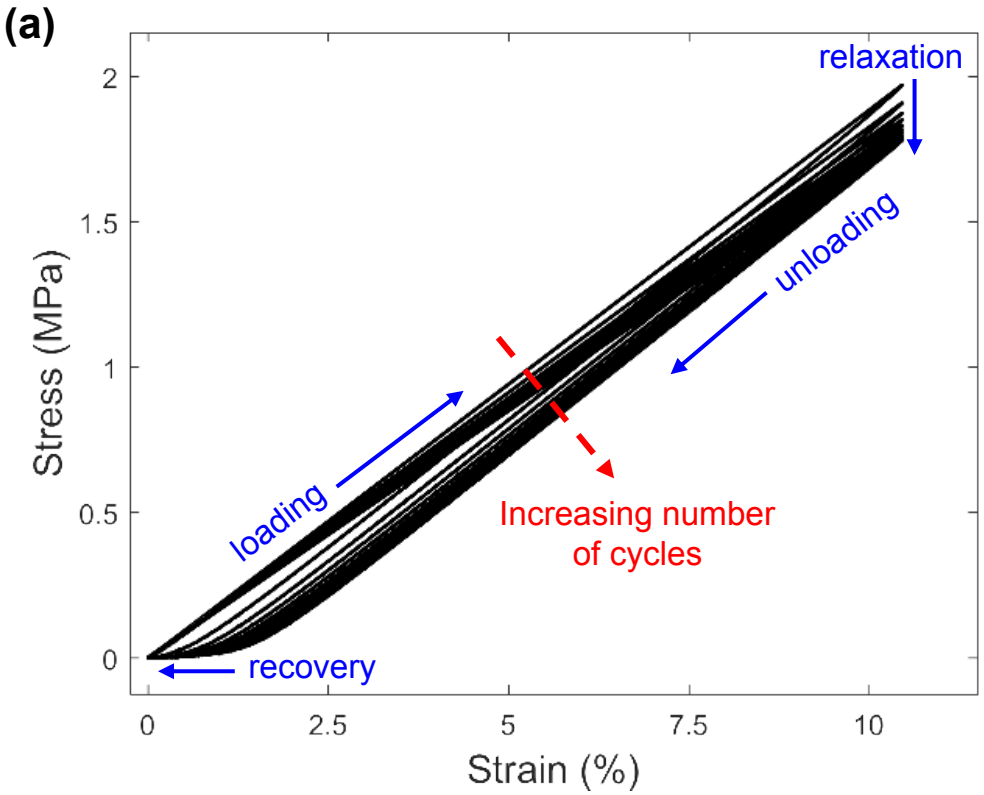
(a)
relaxation
unloading
loading
Increasing number
of cycles
recovery
Stress (MPa)
Strain (%)
0
0.5
1
1.5
2
0
2.5
5
7.5
10

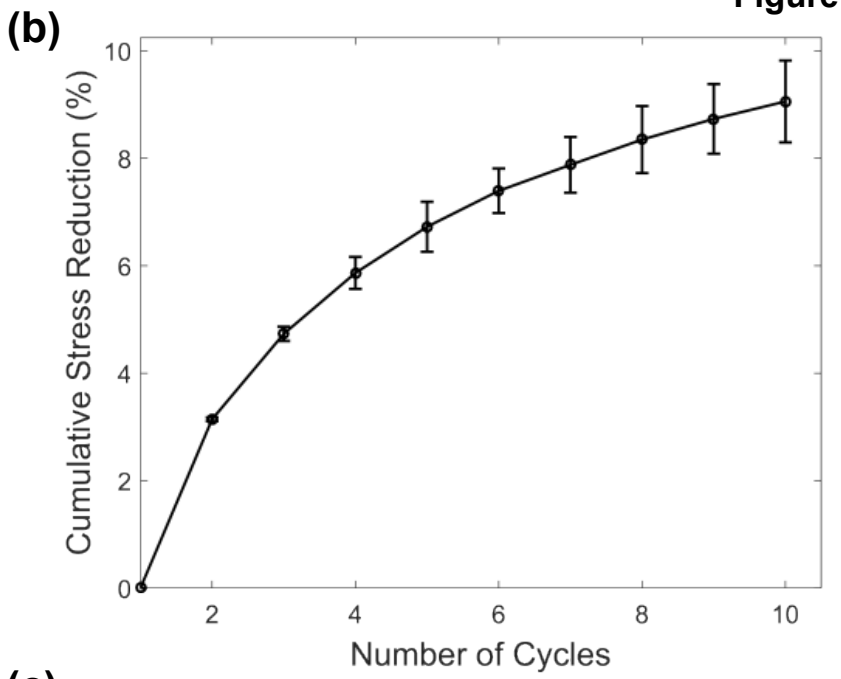
(b)
Cumulative Stress Reduction (%)
Number of Cycles
0
2
4
6
8
10
2
4
6
8
10

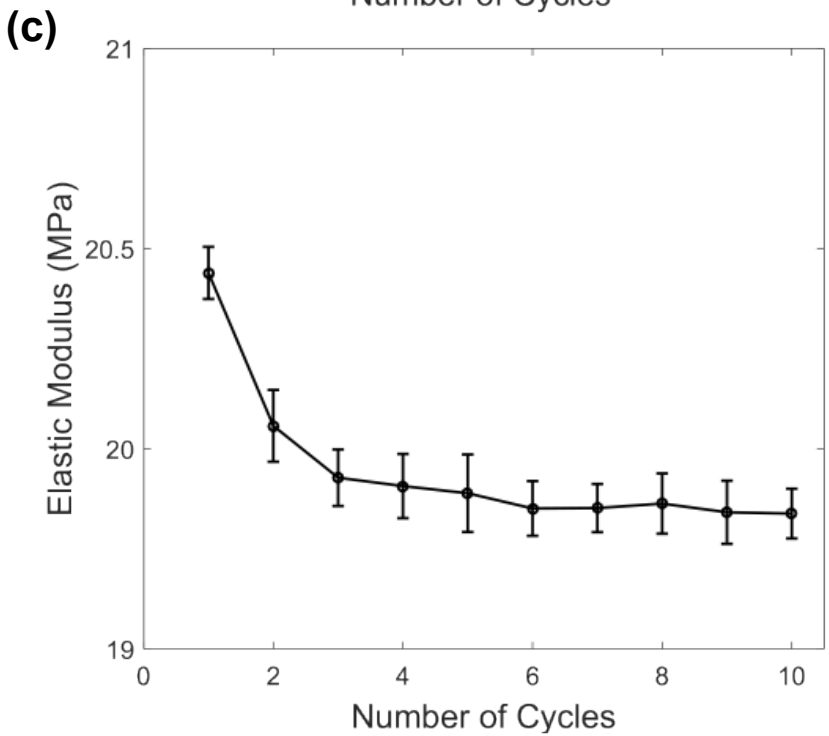
(c)
Elastic Modulus (MPa)
Number of Cycles
19
20
20.5
21
0
2
4
6
8
10

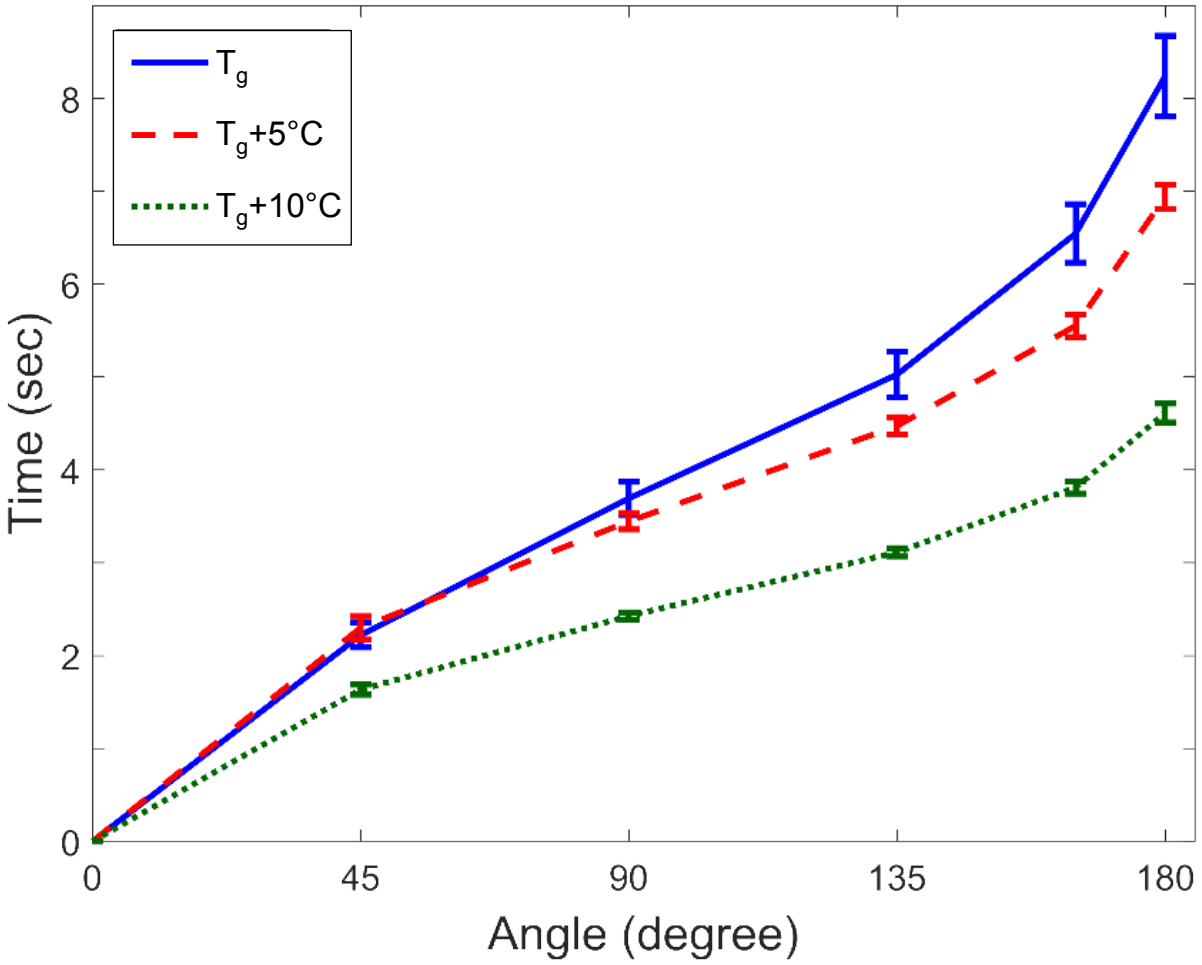
T_g
T_g+5°C
T_g+10°C
Time (sec)
0
2
4
6
8
0
45
90
135
180
Angle (degree)

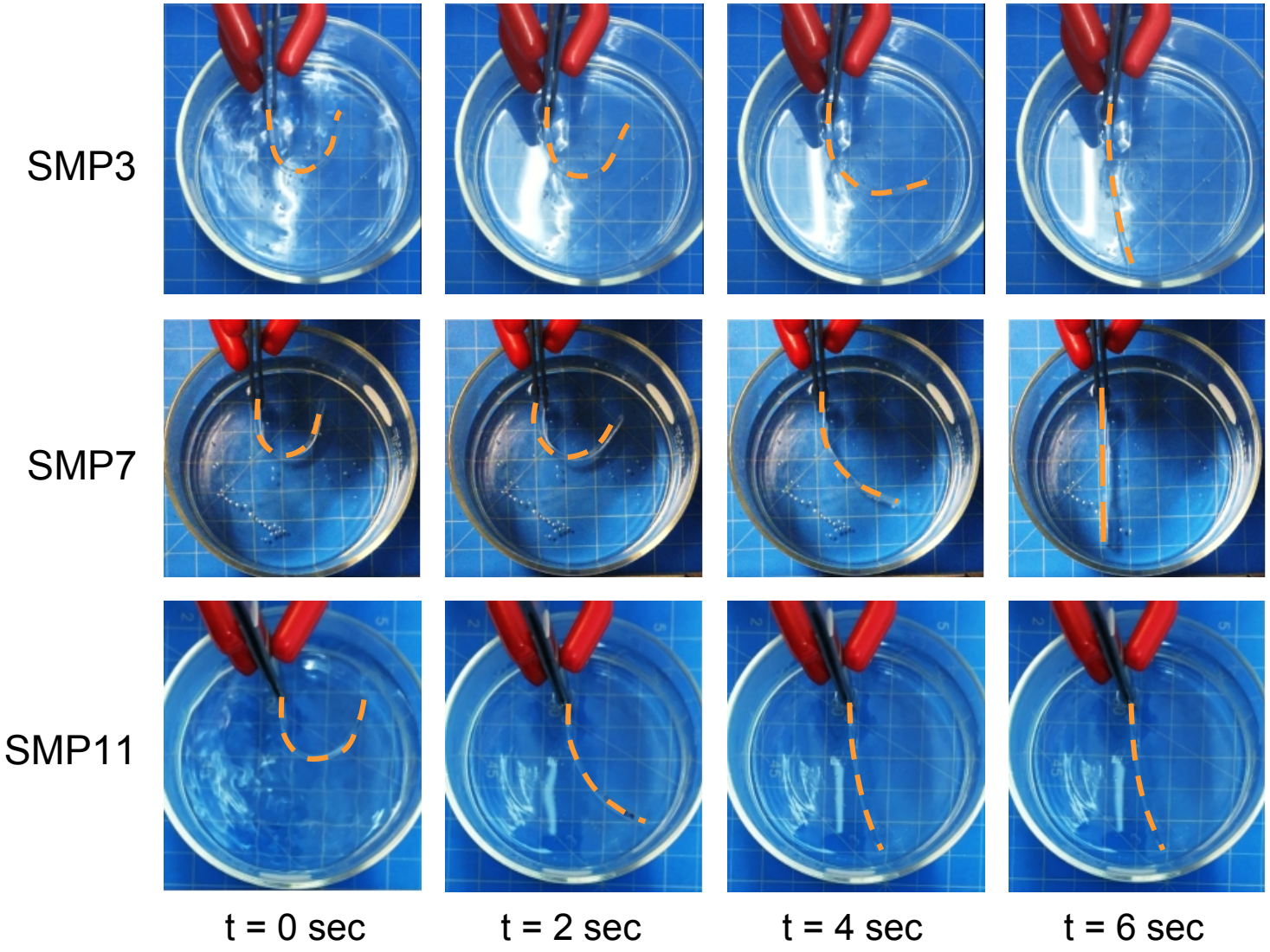
SMP3
SMP7
SMP11
t = 0 sec
t = 2 sec
t = 4 sec
t = 6 sec